Insights into the diagenetic environment of fossil marine vertebrates of the Pisco Formation (late Miocene, Peru) from mineralogical and Sr-isotope data

Gioncada A.[a], Petrini R.[a], Bosio G.[b], Gariboldi K.[a], Collareta A.[a,c], Malinverno E.[b], Bonaccorsi E.[a], Di Celma C.[d], Pasero M.[a], Urbina M.[e], Bianucci G.[a]

[a]*Dipartimento di Scienze della Terra, Università di Pisa, via Santa Maria 53, 56126 Pisa, Italy, anna.gioncada@unipi.it, riccardo.petrini@unipi.it, karen.gariboldi@for.unipi.it, elena.bonaccorsi@unipi.it, marco.pasero@unipi.it, giovanni.bianucci@unipi.it*

[b]*Dipartimento di Scienze dell'Ambiente e della Terra, Università di Milano-Bicocca, Milan, Italy giulia.bosio@unimib.it, elisa.malinverno@unimib.it*

[c]*Dottorato Regionale in Scienze della Terra Pegaso, via Santa Maria 53, 56126 Pisa, Italy, alberto.collareta@for.unipi.it*

[d]*Scuola di Scienze e Tecnologie, Università di Camerino, via Gentile III da Varano, 62032 Camerino, Italy, claudio.dicelma@unicam.it*

[e]*Departamento de Paleontologia de Vertebrados, Museo de Historia Natural de la Universidad Nacional Mayor de San Marcos, Avenida Arenales 1256, Lima 14, Peru, mariourbina01@hotmail.com*

Corresponding author: Anna Gioncada, *anna.gioncada@unipi.it*

Keywords: Sr-isotopes, gypsum, fossilization, Miocene, marine vertebrates, mollusks

Highlights (3-5 max 85 caratteri)

- We study the fossilization environment of the marine vertebrate Pisco Lagerstätte
- We describe textural, mineralogical and Sr-isotope data of post-burial minerals
- Dolomite Sr isotopic ratio agrees with seawater at the time of sedimentation
- Gypsum Sr isotopic ratios suggest an older or modified seawater-derived brine
- Preservation of bones was favored by a suitable diagenetic chemical environment

Abstract

The late Miocene Pisco Formation of Peru is an outstanding example of richness and high-quality preservation of fossil marine vertebrates. In order to reconstruct the fossilization path, we present new textural, mineralogical and Sr-isotope data of diagenetic minerals formed in correspondence of fossil specimens such as marine vertebrates and mollusks. These fossil specimens were found at Cerro los Quesos, in the Ica Desert, within the diatomaceous strata of the Pisco Formation.

Dolomite, gypsum, anhydrite and Mn minerals are the main phases found, while the calcium carbonate originally forming the mollusk valves is replaced by gypsum. An early formation of dolomite and of Mn minerals, triggered by the modifications of the geochemical environment due to organic matter degradation, is suggested by the textural relationships and is confirmed by the Sr isotopic ratio of dolomite, which agrees with that of seawater at the time of sedimentation. Instead, gypsum Sr isotopic ratios indicate a pre-Miocene seawater-derived brine circulating within the sedimentary sequence as a source for Sr. Oxidation of diagenetic sulfide causing a lowering of the pH of porewater is proposed as an explanation for Ca-carbonate dissolution. The diagenetic chemical environment was, nevertheless, favorable to bone preservation.

1. Introduction

The sedimentary strata outcropping in the Ica desert of Peru and belonging to the Pisco Formation (hereinafter: Pisco Fm) have a widely recognized importance for the exceptional abundance in fossil marine vertebrates and for their preservation, deserving the attribution of Fossil-Lagerstätte (Bianucci et al., 2016a, b; Brand et al., 2004; Esperante et al., 2008, 2015; Gariboldi et al., 2015; Gioncada et al., 2016; Marx et al., 2017). The marine vertebrate assemblage, mainly hosted in diatomaceous mudstones, includes toothed and baleen-bearing whales, seals, marine slots, sea turtles, crocodiles, seabirds, and cartilaginous and bony fishes (Bianucci et al., 2016b, and references therein; Bianucci et al., 2016a, c; Collareta et al., 2015, 2017; Di Celma et al., 2017; Gioncada et al., 2016; Lambert et al., 2015, 2017a, b; Landini et al., 2017a, b; Marx et al., 2017; Marx and Kohno, 2016; Stucchi et al., 2015, 2016). Many geological and palaeoecological factors together concurred to create a particular setting favorable to preservation. It has been proposed that, in case of a rapid burial, the establishment of conditions favorable to the formation of dolomite concretions wrapping bone remains had a relevant role in the development of the Pisco Fm Lagerstätte, allowing preservation of exceptionally complete and articulated skeletons and of delicate structures such as baleen bristles (Gariboldi et al., 2015; Gioncada et al., 2016). On the other hand, it is a matter of fact that this large vertebrate fossil record includes many skeletons which are not enclosed in carbonate concretions. Among these, it is possible to find very well preserved specimens, with good articulation and completeness and with highly mineralized bones and even soft tissues (e.g., Marx et al., 2017) as well as scarcely preserved bone remains.

To reconstruct a complete picture of this favorable fossilization environment, it is unavoidable to consider the fossilization path encountered by the vertebrate remains and the role of common diagenetic processes occurred after burial, involving dissolution and precipitation of minerals. Therefore, with the aim to contribute to the reconstruction of the physical and chemical conditions encountered by the vertebrate remains during fossilization, we carried out a Sr-isotope and

mineralogical study of the mineral phases formed after burial in the local environment of selected whale skeletons. We chose vertebrate specimens that are not enclosed by carbonate concretions, because the early-formed dolomite concretions have a strong effect in decreasing the permeability of the bones and of the host sediment, thus limiting the exchanges with the environment and the possibility of mineralization of soft and bone tissues (McCoy et al., 2015). Nearby these specimens, we collected minerals formed after burial and found in veins or filling mollusk valves, and minerals replacing mollusk valves, in order to define the origin of mineralizing fluids and possibly the sequence of mineral formation. The Sr isotopic composition of these mineral phases has been then discussed taking into account the possible sources of Sr. The samples come from the site of Cerro los Quesos (Fig. 1), whose diatomaceous strata are well known from both a geological and paleontological point of view (Bianucci et al., 2016a; Di Celma et al., 2016a). The data discussed in this work provide insights about the fossilization conditions in the Pisco Fm.

2. Geological and stratigraphic framework

The Pisco Basin, in southern Peru, is one of the coastal sedimentary basins formed by trench-parallel structural ridges on the continental shelf and upper slope during Late Cretaceous–early Paleogene time (Thornburg and Kulm, 1981). The East Pisco basin corresponds to the onshore sector of the basin and is bounded to the east by Jurassic-Cretaceous igneous rocks of the Coastal Batholith and to the west by Paleozoic to Jurassic metavolcanic and metasedimentary rocks of the Coastal Cordillera (Fig. 1). The basin is filled by sedimentary units spanning from Eocene to Pliocene and separated by unconformities of regional importance (DeVries, 1998; Dunbar et al., 1990). The Pisco Fm straddles from Miocene to Pliocene with variations in thickness and sedimentary facies in the basin (Di Celma et al., 2017).

Extensive field mapping and sedimentological study of outcrop sections (Di Celma et al., 2016a, b; 2017) have shown that the Pisco Fm is a cyclical sediment unit composed of at least three fining-upward, unconformity-bounded allomembers, designated P0, P1, and P2 from oldest to youngest. Stratigraphically, the three unconformity-bounded units are thought to be equivalent to depositional sequences (Di Celma et al., 2017). Integration of biostratigraphic and tephrochronologic age determinations constrains the ages of the three Pisco sequences within the study area (Di Celma et al., 2017; Gariboldi et al., 2017): based on the $^{40}Ar/^{39}Ar$ ages on tephra beds within the surrounding sediments, a conservative estimate of the age of P0 suggests deposition of these strata between 17.99 ± 0.10 Ma and 9.00 ± 0.02 Ma, whereas diatom biostratigraphy, confirmed by tephrochronology, indicates that strata of the P1 sequence were deposited sometime between 9.5 Ma and 8.9 Ma. Those of the P2 sequence outcropping at Cerro los Quesos are younger than 8.5 Ma and older than 6.71 ± 0.02 Ma based on biostratigraphy and $^{40}Ar/^{39}Ar$ ages.

At Cerro los Quesos (hereinafter: CLQ) the Pisco Fm consists of a basal package of sandstone beds followed by a package of diatomaceous siltstones and mudstones with interbedded volcanic ashes and dolomite layers (Di Celma et al., 2016a; Fig. 1). The strata belong to the P1 and P2 allomembers, and an intraformational unconformity marked by phosphorite nodules has been identified in the lower part of the succession outcropping east of CLQ. Based on sedimentary structures, the depth of the basin during sedimentation was at most 100 m, indicating inner-middle shelf conditions. The measured CLQ section has been divided into six members, from A to F, distinguished on the basis of their characteristic lithofacies (Di Celma et al., 2016a). Member A contains P1 and P2 strata, members B-F correspond to the P2 allomember (Fig. 1).

3. The Cerro los Quesos fossil record

3.1. Marine vertebrates

The late Miocene vertebrate assemblage of CLQ was recently described by Bianucci et al. (2016a) in relation to the detailed local stratigraphic framework of the Pisco Fm provided by Di Celma et al. (2016a). The fossil vertebrate assemblage studied by Bianucci et al. (2016a) is composed of 192 specimens and consists of cetaceans, pinnipeds, crocodiles, birds, bony fishes, sharks, and rays. The cetaceans, including both mysticetes and odontocetes, largely dominate the fossil vertebrate scenario. The baleen-bearing whales account for 42.2% of the identified vertebrate specimens; they are represented by three (or more) species of medium- to large-sized balaenopteroids and, secondarily, by a small-sized cetotheriid (*Piscobalaena nana*). Remains of toothed whales are rather rare but representative of a high number of different taxa, including three species of physeteroids (the macroraptorial *Acrophyseter* sp., *Scaphokogia* sp., and a new *Scaphokogia*-like kogiid), three species of ziphiids (*Chavinziphius maxillocristatus*, *Nazcacetus urbinai*, and a third form inferred on the basis of fragmentary remains), and a single species of phocoenid (cf. *Lomacetus* sp.). Remains of pinnipeds (Phocidae indet.), seabirds (a *Phalacrocorax*-like cormorant), crocodiles (cf. *Piscogavialis* sp.), elasmobranchs (including *Carcharhinus* spp., *Carcharocles megalodon*, *Cosmopolitodus* spp., and *Myliobatis* spp.), and bony fish complete the fossil vertebrate scenario (Bianucci et al., 2016a, c, and references therein; Di Celma et al., 2017; Lambert et al., 2017a). According to Bianucci et al. (2016a), at CLQ, 178 vertebrate specimens (i.e., 92.7% of the total) occur within the largely diatomaceous deposits of member F (sensu Di Celma et al., 2016a; Fig. 1); moreover, 166 vertebrate specimens (i.e., 86.5% of the total) are concentrated in a 40-m-thick interval of sediments spanning from 140 m to 180 m above the base of member C (see the stratigraphic section provided by Bianucci et al., 2016a). Only about one tenth of the fossil vertebrates recognized at CLQ are found embedded within dolomite nodules, a preservation style

which is more frequently observed in the older deposits of the Pisco Fm exposed at Cerro Colorado (Gariboldi et al., 2015). Among those without a concretion envelope, most specimens display localized development of dolomite close to the bone, such as within the skull or between adjacent vertebrae, as described in Gariboldi et al. (2015).

3.2. Invertebrates

The first description of the invertebrate fauna of the Pisco Fm has been realized in the Eighties by de Muizon and DeVries (1985) and by DeVries (1988), and summarized more recently by DeVries and Frassinetti (2003) and DeVries (2007, 2016). A summary of the invertebrate content found in each depositional sequence constituting the Pisco Fm has been presented in Di Celma et al. (2017). The P1 and P2 sequences that crop out at CLQ are characterized by a scarce presence of invertebrate remains and by the predominant lack of bioturbations by macrobenthos. Mollusks are preserved either as gypsum casts of shells or as dolomite or gypsum internal molds. As such, diagnostic characters for species determination are hardly observed. At the bottom of the measured section (Fig. 1), where the P1 sequence crops out, specimens of *Hybolophus* sp. (Bivalvia, Crassatellidae) have been recognized. Few meters above, at the base of the P2 sequence, *Dosinia ponderosa* (Bivalvia, Veneridae) and *Hybolophus* sp. are present, along with gypsum-replaced shells of *Incatella hupei* (Gastropoda, Turritellidae) (Di Celma et al., 2017). A peculiar mollusk concentration is noticed in the upper part of the succession, in correspondence of a few meters thick interval within the fossil-rich portion of member F (Fig. 1), typically occurring as heaps near five partial skeletons of cetaceans. As already stated by Di Celma et al. (2017), none of these specimens is attributable to any genus that usually characterizes the whale-fall communities (Smith et al., 2015). Instead, all the identified specimens belong to the genus *Hybolophus* Stewart, 1930, a semi-infaunal suspension feeder; they have been identified by means of comparison with the morphology of some better preserved specimens from the Pisco Fm.

4. Sampling and analytical procedures

In selecting the specimens of marine vertebrates, we deliberately avoided those completely or largely enclosed in dolomite concretions, because a concretion may approach a closed system with respect to the external sedimentary environment during the diagenetic history, due to its very low permeability and early formation (McCoy et al., 2015; Gariboldi et al., 2015). Among the specimens without an external concretion, we preferred those associated with mollusks, because the minerals forming mollusk casts and internal molds may be of help in defining the sequence of minerals formation during diagenesis. All bones and shells examined in the field and collected for analysis were found in situ, still partially included in the sediment. This excludes that the

association of bivalves with cetaceans was due to recent erosion. The selected specimens of vertebrates, all belonging to cetaceans (C46, C47, O7 and M50, location in the fossil map of Bianucci et al., 2016a), are from the fossil-rich interval within member F of the CLQ stratigraphic section (Fig. 1b). This sedimentary package consists of a homogeneous succession of diatomaceous mudstones, recurrently interrupted by volcanic ash layers representing distal ash-fall of Andean volcanoes. In particular, specimen C47 rests just above a tephra layer. Absolute $^{40}Ar/^{39}Ar$ ages on volcanic ash layers constrain these strata between 6.93±0.09 Ma and 6.71±0.02 Ma (Fig. 1) (Gariboldi et al., 2017).

The samples collected for observations at the micro-scale and for isotopic and mineralogical analysis in correspondence of the four specimens include small fragments of bones, embedding sediment, mollusks, and fracture- and fault-filling veins. In Table 1, field and laboratory descriptions of the specimens of vertebrates and of the sampled materials are reported.

The bone, sediment and mollusk samples were examined under a stereomicroscope, and some mollusks were sectioned to examine the filled internal cavity. Sediment components were inspected with the aid of smear slides for transmitted light microscopy. Fragments were carefully taken from the bivalve specimens and from the bone of fossil vertebrates. Some of them were mounted in resin and prepared as polished sections. After carbon-coating, the fragments were analyzed by scanning electron microscopy (SEM-SEI, Secondary Electron Imaging, and BSEI, back-scattered electrons imaging) and EDS microanalysis, by means of a Philips XL30 equipped with a Dx4i microanalytical device at Earth Science Department of the University of Pisa. Analytical details were 20 kV filament voltage, 5 nA beam current, ZAF correction. XRPD data were collected for the different mollusk casts and internal molds and for gypsum veins. Sampling for mineralogical analysis was carried out with a microdrill apparatus after visual cleaning of sediment from the surface.

For the Sr isotopic analysis, bivalves were selected after visual inspection and following the mineralogical results in order to distinguish and include samples representative of different mineral formation processes (shell replacement, open-space filling). About 10 mg of sample were collected both in the inner shell parts and on superficial layers by means of a microdrill apparatus, taking care to avoid mixing. Sample GB30 was chemically treated using diluted ultrapure HCl on hot plate for dolomite dissolution; the remaining samples were handled for the total dissolution of gypsum. Sr-isotope data were collected by solid-source thermal ionization mass spectrometry (TIMS) using a Finnigan MAT 262 mass spectrometer at the Earth Sciences Department of Sapienza University (Rome, Italy). The reported uncertainties represent in-run statistics at 2-σ confidence level. Repeated analysis of the NBS 987 standard (n= 10) gave an average $^{87}Sr/^{86}Sr$ value of 0.710245(9),

and no correction was applied to the measured ratios for instrumental bias. An external error of ±0.000010 on the measured Sr isotopic composition has been assumed.

5. Results

5.1. Macroscopic observations and mineralogical and microanalytical investigations

The four selected fossil vertebrates, the associated mollusks and the gypsum veins of each outcrop are illustrated by field photos and drawings in Figure 2. A short description with focus on their main taphonomic features is summarized in Table 1, accompanied by a list of the mineral samples from mollusks and from veins collected close to them.

5.1.1. The fossil vertebrates

Specimen O7 is a disarticulated small skeleton with associated bones of an immature (based on unfused epiphyses of vertebrae) phocoenid consisting of a fragment of the skull (rostrum), several vertebrae and several rib fragments. The bones have no concretions and the host sediment does not exhibit color changes indicating diagenetic features.

Specimen M50 is a mysticete (probably balaenopterid) skull, lying in dorsal view, with broken mandibles (Fig. 2A). Based on the equations provided by Lambert et al. (2010), the measured bizygomatic width (ca. 1.5 m) allows an estimation of about 13 m for the original body length. Thanks to the recent erosion that destroyed part of the posterodorsal wall of the braincase, a well-developed dolomite nodule has been observed filling the endocranial cavity (Fig. 2B). Petrographic inspections indicate that the nodule consists of sediment particles (mainly diatom frustules) cemented by microcrystalline (micritic-microsparitic) dolomite, whereas local porosity is filled by dolomite lozenges. The microcrystalline dolomite is spotted by reddish iron oxides and makes transition to a black band, enriched in iron and manganese, close to the cranium bone. The bones of the cranium at the boundary with the nodule show some structures uncertainly recalling microborings.

Specimen C46 consists of several disarticulated but still associated lumbar and caudal vertebrae of an immature (based on unfused vertebral epiphyses) small-sized cetacean (Fig. 2C, D, E, F). These vertebrae are not enclosed in a dolomite concretion, but minor dolomite infilling occurs within bone porosity. For a distance of 10-20 cm from the bones, the sediment hosting the vertebrae is well lithified with respect to the surrounding lithology, as indicated by the emergence of gypsum veins all around, delimiting the specimen (Fig. 2C, D). Outside of this boundary, the sediment becomes reddish-dark gray, and these color variations are here interpreted as variations in the concentration of iron and manganese oxyhydroxides formed during early diagenesis in response to a redox

boundary, by analogy with similar examples documented by Gariboldi et al. (2015).

Specimen C47 consists of few disarticulated vertebrae and fragments of ribs of an adult (based on fused vertebral epiphyses) small-sized cetacean; the bones are still associated (Fig. 2G, H). The cetacean C47 does not exhibit concretions as well; the sediment near the bones is characterized by faint reddish-dark grey boundaries delimiting the specimen, similarly to C46. One juvenile tooth belonging to a lamniform shark (*Cosmopolitodus hastalis)* was found near the ribs, but no shark bite marks have been found on the bones. Inspections of a rib fragment from C47 under a scanning electron microscope (Fig. 4A, B) indicated that the compact bone tissue consists exclusively of calcium phosphate, without any substitution by other minerals. The uniform and dense appearance of the bone tissue under SEM-BSE imaging indicates a rather high degree of apatite mineralization, allowing a good preservation of the bone structures (Fig. 4C). The cortical tissue structures, such as osteons, haversian canals and osteocyte lacunae, are well recognizable and there are no signs of permineralization within bone porosity (Fig. 4C). On the other hand, the external rim of the cortical bone shows an enlargement of haversian canals, possibly by mechanical erosion, and numerous microborings (Fig. 4D), indicating the activity of bone-eating organisms, whose size and distribution recall those designated as "type B" by Gariboldi et al. (2015). Some of the canals and lacunae in the cortical tissue, as well as most of the larger voids of the trabecular tissue of the rib (not shown), contain sparse biogenic (diatoms) and terrigenous sediment particles and are partially filled by bladed gypsum and minor silica and barite.

5.1.2. The mollusks

At CLQ, O7, M50, C46, and C47 are the sole vertebrate specimens that display associated mollusk bivalves. Indeed, mollusks (and, more in general, invertebrate remains) strictly associated to fossil vertebrates are rare in the Pisco Fm. The bivalves collected are not very well preserved and do not maintain their pristine shell, making hard their identification. Comparing some of these bivalves to other specimens from the Pisco Fm in different localities, we observed some similarities that allow us to identify some individuals as belonging to the genus *Hybolophus*.

Hand samples of some of the mollusks are shown in Figure 3, where some of the holes resulting from sampling by microdrilling for isotopic and mineralogical analyses are visible. Identification of the diagenetic minerals by XRPD is reported in Table 2.

The bivalve specimen GB38, found near the vertebrae of O7, is preserved as one single valve replaced by microcrystalline gypsum and partially filled by lithified sediment (Fig. 3A; Tables 1, 2). Other two specimens found associated to this fossil vertebrate show a preserved hinge that allows us to identify these specimens as *Hybolophus* sp.

The specimen GB47 is a replaced single shell found near the specimen M50 (Table 1). The original

Ca carbonate has been replaced by anhydrite and gypsum (Table 2). This bivalve is the only one found near the skull of M50 and is not enough well preserved to be identified.

The mollusks found near the vertebrae of the cetacean specimen C46 are in life-position (Figure 2B, Table 1). This supports that the bivalves lived near the cetacean bones rather than the bone-mollusk association was due to post-mortem transport. Possibly, the partial cementation of the diatomaceous sediment hosting the remains preserved the infaunal bivalves in their original vertical position.

Some of the mollusks associated with C46 are preserved as a perfect carbonate internal mold consisting of a dolomite nodule (Table 2). All the well preserved specimens found near this cetacean remains show similarities in morphology with those of the genus *Hybolophus*. The dolomite mold of GB30 shows the scars of two equal adductor muscles and an intact pallial line, and is partially surrounded by microcrystalline gypsum, probably remnant of the gypsum-replaced shell. Most shells, instead, are apparently entirely replaced and filled by gypsum (e.g. GB35, GB36), showing a slight ornamentation with concentric ribs. XRPD data indicate that gypsum is often accompanied by anhydrite (Table 2). When sectioned, these specimens reveal a core consisting of a dolomite nodule of variable size, with the remaining space filled almost completely by fibrous crystals of gypsum growing inward from the original valves (Fig. 3C). The fibers bend where touching the internal nodule (Fig. 3C). The dolomite internal nodules are yellowish to dark brown in color, and dark brown to black is also the color of the lithified host sediment just outside several mollusks (Fig. 3C, D). SEM-EDS inspections reveal that the dolomite nodules consist mainly of dolomite, as indicated by XRPD data (Table 2), containing scattered biogenic and terrigenous clasts with cavities completely cemented by finely crystallized dolomite (Fig. 4C, D); the blackened portions correspond to concentrations of manganese, probably present as a fine cementing oxydroxide phase together with dolomite (Fig. 4D). Clearly, this situation recalls, at a smaller scale, the Mn-Fe-enriched dolomite concretion filling the cranium of M50 whale specimen (Fig. 2B).

Several mollusk bivalves are associated to the fossil vertebrae and ribs of the cetacean specimen C47 and are mostly entirely replaced and/or filled by gypsum. Among these, the shell GB45 has been sampled for analysis and consists entirely of gypsum (Tables 1, 2). The external part of the shell of this mollusk shows concentric, poorly preserved ribs.

5.1.3. Veins

As regards the gypsum veins collected in correspondence of the specimens O7, M50, C46 and C47, they are all sub-vertical fracture-filling veins with thickness of 0.5-2 cm (see Fig. 3E for an example). Gypsum is fibrous and grows inwards orthogonally to the vein sides. In the studied area we did not find veins with deformed gypsum, which are present elsewhere in the region (Rustichelli

et al., 2016). The XRPD data reported in Table 2 indicate that anhydrite is present together with gypsum in all vein samples. In several samples of veins, the XRPD analyses have detected the presence of variable amounts of quartz, which can be interpreted as belonging to the detrital fraction. The mineralogical analysis has not revealed any other terrigenous or hydrothermal component.

5.2. Sr-isotopes

The $^{87}Sr/^{86}Sr$ ratio measured on mollusks and veins is reported in Table 3.

As regards the mollusks, the dolomite inner mold (mollusk GB30) has $^{87}Sr/^{86}Sr$ ratio of 0.70899; for the gypsum replacing and filling mollusks, the Sr isotopic ratio ranges between 0.70858 and 0.70906, and no systematic differences are observed between external and internal parts and/or among the different fossil specimens. Gypsum from veins is in the range 0.70864 – 0.71111, the most radiogenic values being measured in the O7-GY sample. Despite the limited number of data, the $^{87}Sr/^{86}Sr$ data in mollusks and veins in Table 3, clustering at 0.708925-0,709060 and at 0.708587-0.708766, clearly suggest the contribution of Sr from mainly two isotopically distinct sources, besides additional isotopic heterogeneities.

6. Discussion

6.1. Diagenetic and vein minerals accompanying the fossil marine vertebrates

A sequence of mineral formation and dissolution, occurring after burial and before exposure to supergenic fluids and weathering, can be envisaged for the studied vertebrate and invertebrate specimens.

Although the vertebrate specimens are not enclosed in a carbonate concretion, dolomite formed small nodules inside the internal cavities of the articulate bivalves, as well as a larger nodule inside the endocranial cavity of the M50 baleen whale skull. The microcrystalline texture of dolomite, together with its occurrence in nearly closed, protected environments, having abundant decaying organic matter and scarce exchange with the surrounding seawater (the still articulated and closed shells of bivalves, the endocranial cavity, and in some cases the trabecular cavities of bones), strongly suggest that dolomite formed with a localized process analogous to that forming carbonate concretions enclosing fossil specimens. The latter process has been described as linked to anaerobic organic matter decay through bacterial sulfate reduction, providing the alkalinity for carbonate precipitation (Berner, 1981; Gariboldi et al., 2015; McCoy et al., 2015; Yoshida et al., 2015). In particular, for dolomite concretions, biomediated sulfate reduction has been proposed to counteract the inhibiting effect of sulfate on dolomite primary precipitation in a marine environment (Baker

and Kastner, 1981).

Outside these protected environments (the closed shells of bivalves and the endocranial cavities of vertebrates), the development of dolomite is limited: dolomite was found in the sediment enclosing the mollusks associated to C46, whose partial consolidation is also suggested by the arrangement of gypsum veins emergences all around the specimen (Fig. 2C, D). The scarce formation of dolomite around the bone and mollusks may indicate an insufficient sulfate reduction due to a steady availability of sulfate-bearing and oxygenated seawater, allowing aerobic organic matter oxidation. This suggests that the carcasses of the studied cetaceans remained exposed on the seafloor, instead of being rapidly buried, while decay occurred. The disarticulation of the skeleton could have mostly occurred during this period of time.

Iron oxides and manganese oxide minerals accompany dolomite within and around the mollusks and in the endocranial nodule (Fig. 2B, 3 and 4). The textural relationships indicate that, in correspondence of the studied mollusks, Mn precipitation always preceded gypsum (an example in Fig. 3D). The textural relationships with dolomite, instead, are controversial. These observations, joined to the fact that these Mn concentrations are not governed by permeability and neither line voids nor form dendritic growth structures on surfaces, does not support a late formation for Mn minerals (Pfretzschner and Tutken, 2011). Instead, in our case we can propose that Mn concentration next and within the dolomite nodules in mollusks and endocranial cavities was related to the modified geochemical conditions induced by organic matter decay. In fact, Mn and Fe reduction are among the first mechanisms for anaerobic organic matter degradation, after the exhaustion of available oxygen, and this process could have increased the concentration of Mn and Fe in porewater. With the involvement of porewater sulfate as an oxidizing agent for organic matter, and the consequent production of sulfide, iron was fixed as iron sulfides. Additional sulfur could be released, also, by decaying collagen (Pfretzschner, 2004). Evidence for processes of iron sulfide formation at CLQ is provided by the common finding of ghosts of framboidal pyrite (Gariboldi et al., 2015). Manganese, instead, is not influenced by sulfidic conditions. Its precipitation could be caused by the increase in alkalinity due to sulfate reduction, or to the resumed exchange with oxygenated seawater at sea bottom after the exhaustion of organic matter.

Since, in some cases, the dolomite concretion has completely filled the internal cavity of the articulated shells of the bivalves, forming an internal mold replicating the internal features, it is possible to assume that the calcium carbonate shell was still present when dolomite formed. However, no or negligible calcium carbonate is currently present in the studied samples, where biogenic calcite is replaced by gypsum. The above depicted processes allow to suggest a possible explanation for calcite dissolution. In fact, the resuming oxygenated conditions around and within bivalves, besides causing the precipitation of Mn, caused the oxidation of the previously formed

iron sulfides, or of the sulfide produced by sulfate reduction, leading to a reduction of pH (Coleman et al., 1985). The resulting local acidification can be proposed as a cause for the dissolution of the calcium carbonate shells, similarly to what has been proposed in other carbonate-bearing sedimentary environments (Lin et al., 2016; Pirlet et al., 2010). The same authors suggest that the resulting elevated Ca concentration in porewater and the availability of sulfate can also play a role in the formation of authigenic gypsum; however, in our case, this mostly disagrees with the Sr isotopic composition of gypsum (see below). Moreover, although it cannot be excluded that part of the gypsum forming the mollusks was early diagenetic (in some cases, more than one phase of gypsum is suggested by inspection of texture within replaced mollusks), a formation of gypsum extended to late diagenesis at CLQ is indicated by the abundant veins and cavities filled by gypsum with fibrous texture, which would not be explained by the above process alone.

6.2. Constraints from Sr isotopic composition of minerals

The $^{87}Sr/^{86}Sr$ isotope-ratio in the world's oceans has varied through geological time, and the Sr isotopic composition may be used, in principle, to date marine minerals, to correlate stratigraphic sections of marine deposits and to define the biostratigraphic and paleoenvironmental framework (Faure and Mensing, 2005). The basic assumption for the application of the Sr-isotopes method to determine the specific age of Sr-bearing marine mineral phases is that the ocean Sr isotopic composition is homogeneous; this is supported by the Sr residence time in the oceans that is about three orders of magnitude longer compared with the time required by the oceans to mix, allowing the formation of a homogeneous Sr-isotope reservoir within ±0.00002 of the $^{87}Sr/^{86}Sr$ ratio (De Paolo and Ingram, 1985). However, the Sr isotopic pattern of seawater during the Phanerozoic is complex, in some cases resulting in ambiguous dating. Exception is the monotonic and steep increase of the Sr isotopic composition of seawater since the Oligocene to the present day, allowing reliable numerical ages to be obtained in this time-span (McArthur et al., 2001). This can be done through the analysis of marine mollusks, assuming that the $^{87}Sr/^{86}Sr$ ratio of seawater is preserved in the carbonate shell since the time of incorporation and early diagenesis.

In the studied mollusk samples, the original carbonate shell is not preserved and has been replaced by gypsum; the inner mold is made of dolomite. Following the Sr-isotope chronostratigraphy (McArthur et al., 2001), the $^{87}Sr/^{86}Sr$ ratio measured in the dolomite filling of the GB30 specimen (C46 fossil whale) yields a numerical age of 6.2±0.4 Ma. Such date is consistent with the absolute radiometric age of 6.93±0.09 and 6.71±0.02 Ma obtained by $^{40}Ar/^{39}Ar$ analyses (Di Celma et al., 2016a) on biotite from tephra layers about 10 m below and 40 m above, respectively (Fig. 1). This overall correspondence is in agreement with a formation of dolomite as an early seawater precipitate during the Messinian, favored by the local increase of porewater alkalinity due to

organic matter oxidation and sulfate reduction (Bontognali et al., 2013; Vasconcelos et al., 1995), confirming the hypothesis of Gariboldi et al. (2015) of early dolomite precipitation for the formation of the nodules wrapping fossil marine vertebrates in the Pisco Fm. With similar mechanisms, the occurrence of dolomite layers in sediments from the Peru Margin has been related to the conditions established at shallow depth below the seafloor during early diagenesis, at the sulfate reduction-methanogenesis boundary in the sedimentary column (Meister et al., 2007).

The $^{87}Sr/^{86}Sr$ ratio of gypsum from mollusks deviates from the isotopic value of dolomite, towards a lower isotopic composition (with the exception of sample GB45B which is slightly higher), in some cases overlapping with the $^{87}Sr/^{86}Sr$ ratio measured in gypsum veins. To understand these results, it is necessary to discuss the possible sources of Sr responsible for the isotopic composition of gypsum, and the mechanism of gypsum formation. Evaporation of seawater is the most common, although not the sole, mechanism of formation for gypsum in marine sediments (Horeau et al., 2011). In the hypothesis of seawater evaporation, calcite precipitation causes a chemical divide in the water chemistry (Drever, 1998) allowing gypsum to form when all carbonate has been removed. A Sr isotopic composition of gypsum close to dolomite would have been expected if the isotopic equilibrium with evaporating seawater was attained. Similarly, a Sr isotopic composition close to dolomite would have been expected if all the gypsum was related to an early oxidation of sulfide to sulfate. The observed disequilibrium requires an isotopically distinct source for Sr. Due to the high Sr content of seawater compared to freshwaters, it is unlikely that river inputs with different Sr-isotope ratio were able to cause these deviations. A possible explanation is that the $^{87}Sr/^{86}Sr$ ratio of gypsum reflects a pre-Miocene seawater-derived brine as a source for Sr, characterized by a lower $^{87}Sr/^{86}Sr$ ratio, entrapped in the sediment pores of the shelf sites for a long time (Kastner et al., 1990; Meister et al., 2007). The migration of these brines and their interaction with the sediments, possibly modifying their isotopic composition, is able to explain the variability of the gypsum Sr-isotope data and is in agreement with the observation that gypsum formation post-dates of an undetermined interval of time the early diagenetic minerals (dolomite, Mn minerals). A role for old evaporitic layers in providing a saline fluid component to these brines cannot be excluded. Despite the common occurrence of gypsum-filled faults and fractures (Rustichelli et al, 2016), no evaporitic successions or layers of primary gypsum have been observed along the sedimentary sections exposed at CLQ (Di Celma et al., 2016a); however, in the Pisco Fm, evaporites have been reported by Marocco and de Muizon (1988), indicating that local evaporitic basins formed during sedimentation of the Pisco Fm.

The upward migration of the saline fluids would control the formation of most gypsum veins. Only one vein distinguishes for a significantly higher Sr-radiogenic signature with respect to the remaining samples and falling outside the range of marine waters. This might reflect a contribution

457 from hydrothermal fluids where volcanic SO_2 is the primary driver for sulfate production, and Ca
458 (and Sr) originated from the alteration of Ca-bearing silicate minerals and volcanic glass in Mio-
459 Pliocene ignimbrites, having $^{87}Sr/^{86}Sr$ that reaches 0.7110 (Mamani et al., 2010).
460 Some considerations can be done regarding the occurrence of anhydrite. Anhydrite has been
461 revealed by XRPD analysis of veins and of mollusks, along with gypsum (Table 2). Anhydrite is
462 favored in respect to gypsum by pressure conditions sufficient for dehydration, by temperature
463 (above 55°C at 1 atm) and by salinity of the solution. The transition of gypsum to anhydrite due to
464 the sedimentary overburden requires at least 0.5-1 km of load (Jowett et al., 1993), but, since the
465 maximum thickness of the entire Pisco Fm is less than 1 km (Dunbar et al., 1990), we can exclude
466 pressure as a factor explaining the occurrence of anhydrite, as already suggested by Rustichelli et al.
467 (2016). These authors suggest weathering in the hot and arid desert climate as a cause for the
468 presence of anhydrite in the outcropping veins of the Pisco Fm. Alternatively, we propose that the
469 circulation of high-salinity brines in the subsoil could have favored the partial dissolution of
470 gypsum and precipitation of anhydrite, prior to exhumation. Anhydrite could have survived without
471 rehydrating to gypsum due to the arid environment encountered after exhumation (see Pueyo et al.,
472 2001 for anhydrite associated to evaporitic gypsum in the Atacama Desert).
473
474 **6.3. Implications for the preservation of vertebrate remains**
475 It has been ascertained that, in several cases, the preservation of complete and articulated
476 vertebrates in the Pisco Fm was favored by the formation of dolomite concretions in an early
477 diagenetic stage (Gariboldi et al., 2015; Gioncada et al., 2016). However, the observation that the
478 Pisco abundance of fossil vertebrates is also due to many skeletons preserved without a nodule, in
479 poorly lithified sediments (e.g., Marx et al., 2017), suggests that the diagenetic environment was
480 overall favorable to the preservation of the bones both during the early diagenetic stage and
481 subsequently, although recent erosion limited the chance to find specimens with high completeness
482 and articulation out of the nodules.
483 The preservation of bones of marine vertebrates through diagenesis strongly relies on the early
484 diagenetic environment favoring the mineralization process of bone tissues and counteracting
485 possible processes of bone dissolution during further diagenesis (Pfretzschner, 2004; Keenan,
486 2016). Early diagenesis of bones is characterized, at first, by destructive processes related to the
487 intense microbial activity and to decay of collagen, then by the preserving mechanisms allowing
488 bone fossilization through hydroxylapatite recrystallization to a more stable Ca-phosphate mineral
489 phase (Pfretzschner, 2004; Piga et al., 2011; Trueman, 1999; Trueman et al., 2004; Keenan, 2016).
490 The minerals and features identified in correspondence of the vertebrate and invertebrate remains
491 and the preliminary Sr-isotope data allow to constrain the early diagenetic processes occurred in

correspondence of these vertebrate remains of CLQ. The bones of the studied specimens display evidence of degradation (microborings) which occurred early, due to the action of bacterial activity on carcasses, and resulted in a remarkable weakening of the outer part of the compact bone (Fig. 4B). On the other hand, the internal structures of the compact bone are well preserved by Ca-phosphate (Fig. 4A), highlighting the occurrence of processes of bone mineralization accomplished through chemical exchanges of bone with seawater during early diagenesis, concomitantly to the degradation of collagen. Sulfate reduction and manganese reduction (among other mechanisms of organic matter oxidation) are testified respectively by the presence of dolomite and manganese minerals in correspondence of the fossil invertebrates, but the formation of these minerals does not affect the bones unless in the most closed environments (endocranium). The further history of these vertebrate remains is registered only in gypsum and very minor barite filling the larger cavities of bones, and other evidence of bone tissue degradation, such as chemical attack or dissolution, or replacement by common late minerals such as calcite, Fe-Mn oxides, silica, have not been detected. This is in agreement with the porewaters being dominated by the concentrated brines migrating in the sedimentary successions, maintaining a geochemical environment favorable to apatite crystallization in time.

7. Conclusions

The elevated concentration of fossil marine vertebrates at CLQ, along with an exceptional preservation of bones both with and without carbonate concretions, suggests that the diagenetic environment of the Pisco Fm was overall favorable to the preservation of bones. The study of the bone remains and associated fossilized mollusks in the diatomaceous strata of the Pisco Fm at CLQ gives insights into the fossilization path, contributing to the understanding of the preserving environment. In particular, the temporal sequence of diagenetic minerals displayed by the mollusks helps to understand the geochemical environment where bone fossilization occurred.

Dolomite and Mn minerals formed with different mechanisms during the early diagenesis, following the Mn and sulphate reduction processes related to the decay of organic matter in environments with limited supply of oxygenated seawater, such as inside the internal cavity of articulated mollusk shells and the endocranial cavity of whale's skull. The Sr isotopic composition of dolomite confirms an early formation from late Miocene seawater. Subsequently, but still during the early diagenesis, oxidation of the diagenetic sulfide may have lowered the pH enough to dissolve the bivalve shells, explaining the current lack of calcite. The void left was then filled by gypsum.

Differently from dolomite, the Sr isotopic data on gypsum sampled close to fossil vertebrates, as veins and as mollusk replacement and filling, deviate from the isotopic value of seawater at the time

of sedimentation towards a lower isotopic composition. This indicates that the late Miocene diatomaceous sediments of the Pisco Fm were interested by circulation of fluids deriving from an older seawater, replicating the situation that is currently observed for the present Peruvian shelf sediments. The occurrence of anhydrite formed at the expense of gypsum supports the involvement of concentrated brines circulating within these sedimentary sequences.

Although the compact bones without concretion is weakened, in the external part of it, by the presence of microborings formed by the bone-eating bacterial activity, the bone tissue shows a rather good apatite mineralization. Thus, the sedimentary sequences permeated by the above mentioned concentrated brines seem to have maintained a geochemical environment favorable to apatite stability in time.

Acknowledgements

The authors are grateful to F. Colarieti and C. Gini for assistance during analytical data collection. A particular thank to D. Basso and T.J. DeVries for the comments and advices on fossil mollusks of the Pisco Fm. We also thank Rafael Varas-Malca and Walter Aguirre for their help during the fieldtrips at Cerro Colorado and Cerro los Quesos. Two anonymous reviewers are thanked for their comments. This work was supported by the University of Pisa PRA_2015_0028 grant to M. Pasero, the University of Pisa PRA_2017_0032 grant to G. Bianucci, and by the PRIN (Progetti di Ricerca di Interesse Nazionale) Project 2012YJSBMK EAR-9317031 to G. Bianucci.

References

Baker, P.A., Kastner, M., 1981. Constraints on the formation of sedimentary dolomite. Science, 213, 214–216.

Berner, R.A., 1981. Authigenic mineral formation resulting from organic matter decomposition in modern sediments. Fortschritte der Mineralogie, 59, 117–135.

Bianucci, G., Di Celma, C., Collareta, A., Landini, W., Post, K., Tinelli, C., de Muizon, C., Bosio, G., Gariboldi, K., Gioncada, A., Malinverno, E., Cantalamessa, G., Altamirano-Sierra, A., Salas-Gismondi, R., Urbina, M., Lambert, O., 2016a. Fossil marine vertebrates of Cerro Los Quesos: Distribution of cetaceans, seals, crocodiles, seabirds, sharks, and bony fish in a late Miocene locality of the Pisco Basin, Peru. Journal of Maps, 12, 1037–1046.

Bianucci, G., Di, Celma C., Landini, W., Post, K., Tinelli, C., de Muizon, C., Gariboldi, K., Malinverno, E., Cantalamessa, G., Gioncada, A., Collareta, A., Salas-Gismondi, R., Varas-Malca, R.M., Urbina, M., Lambert, O., 2016b. Distribution of fossil marine vertebrates in Cerro Colorado,

561 the type locality of the giant raptorial sperm whale Livyatan melvillei (Miocene, Pisco Formation,
562 Peru). Journal of Maps, 12, 543–557.

563 Bianucci, G., Di Celma, C., Urbina, M., Lambert, G., 2016c. New beaked whales from the late
564 Miocene of Peru and evidence for convergent evolution in stem and crown Ziphiidae (Cetacea,
565 Odontoceti). PeerJ 4:e2479. DOI 10.7717/peerj.2479.

566 Bianucci, G., Lambert, O., Post, K., 2010. High concentration of long-snouted beaked whales
567 (genus Messapicetus) from the Miocene of Peru. Palaeontology, 53, 1077–1098.

568 Bontognali, T.R.R., McKenzie J.A., Warthmann, R.J., Vasconcelos, C., 2014. Microbially
569 influenced formation of Mg-calcite and Ca-dolomite in the presence of exopolymeric substances
570 produced by sulphate-reducing bacteria. Terra Nova, 26, 72-77.

571 Brand, L.R., Esperante, R., Chadwick, A.V., Poma Porras, O., Alomía, M., 2004. Fossil whale
572 preservation implies high diatom accumulation rate in the Miocene–Pliocene Pisco Formation of
573 Peru. Geology, 32, 165–168.

574 Coleman, M.L., Berner, R.A., Durand, B., Meadows, P.S., Eglinton, G., 1985. Geochemistry of
575 Diagenetic Non-Silicate Minerals Kinetic Considerations. Philosophical Transaction of the Royal
576 Society A, 315, 39-56, DOI: 10.1098/rsta.1985.0028.

577 Collareta, A, Landini, W., Chacaltana, C., Valdivia, W., Altamirano-Sierra, A., Urbina, M.,
578 Bianucci, G., 2017. A well preserved skeleton of the fossil shark *Cosmopolitodus hastalis* from the
579 late Miocene of Peru, featuring fish remains as fossilized stomach contents. Rivista Italiana di
580 Paleontologia e Stratigrafia (Research in Paleontology and Stratigraphy), 123, 11-22.

581 Collareta, A., Landini, W., Lambert, O., Post, K., Tinelli, C., Di Celma, C., Panetta, D., Tripodi, M.,
582 Salvadori, P.A., Caramella, D., Marchi, D., Urbina, M., Bianucci, G., 2015. Piscivory in a Miocene
583 Cetotheriidae: first record of fossilized stomach content for an extinct baleen-bearing whale. The
584 Science of Nature, 102, article no. 70.

585 De Paolo, D.J., Ingram, B.L., 1985. High-resolution stratigraphy with strontium isotopes. Science,
586 227, 938–941.

587 DeVries, T.J., 1988. Molluscs of the Pisco Basin. Pisco Basin Guidebook. In: R. B. Dunbar and P.
588 A. Baker (Editors), Cenozoic Geology of the Pisco Basin, IGCP, 156, 127-134.

589 DeVries, T.J., 2007. Cenozoic Turritellidae (Gastropoda) from Southern Peru. Journal of
590 Paleontology, 81, 331-351.

591 DeVries, T.J., 2016. Fossil Cenozoic crassatelline bivalves from Peru: New species and generic
592 insights. Acta Palaeontologica Polonica, 61, 661-688.

593 DeVries, T.J., Frassinetti, D., 2003. Range extensions and biogeographic implications of Chilean
594 Neogene mollusks found in Peru. Boletín del Museo Nacional de Historia Natural, Chile, 52, 119-
595 135.

596 Di Celma, C., Malinverno, E., Bosio, G., Collareta, A., Gariboldi, K., Gioncada, A., Molli, G.,
597 Basso, D., Varas-Malca, R., Pierantoni, P.P., Villa, I.M., Lambert, O., Landini, W., Sarti, G.,
598 Cantalamessa, G., Urbina, M., Bianucci, G., 2017. Sequence stratigraphy and palaeontology of the
599 Upper Miocene Pisco Formation along the western side of the lower Ica Valley (Ica Desert, Peru).
600 Rivista Italiana di Paleontologia e Stratigrafia (Research in Paleontology and Stratigraphy), 123,
601 255-274.

602 Di Celma, C., Malinverno, E., Cantalamessa, G., Gioncada, A., Bosio, G., Villa, I.M., Gariboldi, K.,
603 Rustichelli, A., Pierantoni, P.P., Landini, W., Tinelli, C., Collareta, A., Bianucci, G., 2016a.
604 Stratigraphic framework of the late Miocene Pisco Formation at Cerro Los Quesos (Ica Desert,
605 Peru). Journal of Maps, 12, 1020-1028.

606 Di Celma, C., Malinverno, E., Gariboldi, K., Gioncada, A., Rustichelli, A., Pierantoni, P.P.,
607 Landini, W., Bosio, G., Tinelli, C. Bianucci, G., 2016b. Stratigraphic framework of the late
608 Miocene to Pliocene Pisco Formation at Cerro Colorado (Ica Desert, Peru). Journal of Maps, 12,
609 515-557.

610 Drever, J. I., 1998. The geochemistry of natural waters. Vol. 437. Englewood Cliffs: prentice Hall.

611 Dunbar, R.B., Marty, R.C., Baker, P.A., 1990. Cenozoic marine sedimentation in the Sechura and
612 Pisco basins, Peru. Palaeogeography, Palaeoclimatology, Palaeoecology, 77, 235-261.

613 Esperante, R., Brand, L.R., Chadwick, A.V., Poma, O., 2015. Taphonomy and paleoenvironmental
614 conditions of deposition of fossil whales in the diatomaceous sediments of the Miocene/Pliocene
615 Pisco Formation, southern Peru - a new Fossil-Lagerstätte. Palaeogeography, Palaeoclimatology,
616 Palaeoecology, 417, 337-370.

617 Esperante, R., Brand, L.R., Nick, K.E., Poma, O., Urbina, M., 2008. Exceptional occurrence of
618 fossil baleen in shallow marine sediments of the Neogene Pisco Formation, Southern Peru.
619 Palaeogeography, Palaeoclimatology, Palaeoecology, 257, 344–360.

620 Faure, G., Mensing, T., 2005. Isotopes. Principles and Applications. John Wiley & Sons, New
621 Jersey, 897 pp.

622 Gariboldi, K., Bosio, G., Malinverno, E., Gioncada, A., Di Celma, C., Villa, I.M., Urbina, M.,
623 Bianucci, G., 2017. Biostratigraphy, geochronology and sedimentation rates of the upper Miocene
624 Pisco Formation at two important marine vertebrate fossil-bearing sites of southern Peru.

Newsletters on Stratigraphy, doi: 10.1127/nos/2017/0345.

Gariboldi, K., Gioncada, A., Bosio, G., Malinverno, E., Di Celma, C., Tinelli, C., Cantalamessa, G., Landini, W., Urbina, M., Bianucci, G., 2015. The dolomitic nodules enclosing fossil marine vertebrates in the East Pisco Basin, Peru: field and petrographic insights into their genesis and role in preservation. Palaeogeography, Palaeoclimatology, Palaeoecology, 438, 81-95.

Gioncada, A., Collareta, A., Gariboldi, K., Lambert, O., Di Celma, C., Bonaccorsi, E., Urbina, M., Bianucci, G., 2016. Inside baleen: Exceptional microstructure preservation in a late Miocene whale skeleton from Peru. Geology, 44, 839-842.

Hoareau, G., Monnin, C., Odonne, F., 2011. The stability of gypsum in marine sediments using the entire ODP/IODP porewater composition database. Marine Geology, 279, 87-97.

Jowett, E.C., Cathles III, L.M., Davis, B.W., 1993. Predicting depths of gypsum dehydration in evaporitic sedimentary basin. AAPG Bulletnin, 77, 402-413

Kastner, M., Elderfield, H., Martin, J.B., Suess, E., Kvenvolden, A., Garrison, R.E., 1990. Diagenesis and interstitial water chemistry at the Peruvian continental margins - Major constituents and strontium isotopes. In: E. Suess and R. von Huene (Editors), Initial reports of the Ocean Drilling Program, 112B, 413-440.

Keenan, S.W. 2016. From bone to fossil: A review of the diagenesis of bioapatite. American Mineralogist, 101, 1943-1951.

Lambert, O., Bianucci, G., Muizon, C. de., 2017a. Macroraptorial sperm whales (Cetacea, Odontoceti, Physeteroidea) from the Miocene of Peru. Zoological Journal of the Linnean Society, 179, 404-474.

Lambert, O., Bianucci, G., Post, K., Muizon, C. de, Salas-Gismondi, R., Urbina, M., Reumer, J., 2010. The giant bite of a new raptorial sperm whale from the Miocene epoch of Peru. Nature, 466, 105-108.

Lambert, O., Bianucci, G., Urbina, M., Geisler, J.H., 2017b. A new inioid (Cetacea, Odontoceti, Delphinidae) from the Miocene of Peru and the origin of modern dolphin and porpoise families. Zoological Journal of the Linnean Society, 179, 919-946.

Lambert, O., Collareta, A., Landini, W., Post, K., Ramassamy, B., Di Celma, C., Urbina, M., Bianucci, G., 2015. No deep diving: evidence of predation on epipelagic fish for a stem beaked whale from the late Miocene of Peru. Proceedings of the Royal Society of London Part B: Biological Sciences, 282, 20151530.

Landini, W., Collareta, A., Pesci, F., Di Celma, C., Urbina, M., Bianucci, G., 2017a. A secondary

nursery area for the copper shark *Carcharhinus brachyurus* from the late Miocene of Peru. Journal of South American Earth Sciences, doi: 10.1016/j.jsames.2017.07.003.

Landini, W., Altamirano-Sierra, A., Collareta, A., Di Celma, C., Urbina, M., Bianucci, G., 2017b. The late Miocene elasmobranch assemblage from Cerro Colorado (Pisco Formation, Peru). Journal of South American Earth Sciences, 73, 168-190.

Lin, Q., Jiasheng, W., Thomas J. A., Pibo, S., Gaowei, H., 2016. Formation mechanism of authigenic gypsum in marine methane hydrate settings: Evidence from the northern South China Sea. Deep-Sea Research I, 115, 210–220.

Mamani, M., Wörner, G., Sempere, T., 2010. Geochemical variations in igneous rocks of the Central Andean orocline (13° S to 18° S): Tracing crustal thickening and magma generation through time and space. Geological Society of America Bulletin, 122, 162-182.

Marocco, R., Muizon, C. de, 1988. Le Bassin Pisco, bassin cénozoïque d'avant arc de la côte du Pérou central: Analyse géodynamique de son remplissage. Géodynamique, 3, 3-19.

Marx, F.G., Collareta, A., Gioncada, A., Post, K., Lambert, O., Bonaccorsi, E., Urbina, M., Bianucci, G., 2017. How whales used to filter: exceptionally preserved baleen in a Miocene cetotheriid. Journal of Anatomy, doi: 10.1111/joa.12622.

Marx, F.G., Kohno, N., 2016. A new Miocene baleen whale from the Peruvian desert. Royal Society Open Science, 3, 160542.

McArthur, J.M., Howarth, R.J., Bailey, T.R., 2001. Strontium isotope stratigraphy: LOWESS version 3. Best-fit line to marine Sr-isotope curve for 0 to 509 Ma and accompanying look-up table for deriving numerical age. Look-up table. The Journal Geology, 109, 155-169.

McCoy, V.E., Young, R.T., and Briggs, D.E.G., 2015. Factors controlling exceptional preservation in concretions: Palaios, 30, 272–280, doi:10.2110/palo.2014.081.

Meister, P., Mckenzie, J. A., Vasconcelos, C., Bernasconi, S., Frank, M., Gutjahr, M., Schrag, D. P., 2007. Dolomite formation in the dynamic deep biosphere: results from the Peru Margin. Sedimentology, 54, 1007-1032.

Muizon, C. de., 1988. Les vertébrés fossiles de la Formation Pisco (Pérou). Troisième partie: Les Odontocètes (Cetacea, Mammalia) du Miocène. Travaux de l'Institut Français d'Etudes Andines. 42, 1–244.

Muizon C. de, DeVries, T.J., 1985. Geology and paleontology of late Cenozoic marine deposits in the Sacaco area (Peru). Geologische Rundschau, 74, 547-563.

688 Pfretzschner, H. U., 2004. Fossilization of Haversian bone in aquatic environment. C. R. Palevol, 3,
689 605-616.

690 Pfretzschner, H.-U., Tütken T., 2011. Rolling bones–Taphonomy of Jurassic dinosaur bones
691 inferred from diagenetic microcracks and mineral infillings. Palaeogeography, Palaeoclimatology,
692 Palaeoecology, 310, 117-123.

693 Piga, G., Santos-Cubedo, A., Brunetti, A., Piccinini, M., Malgosa, A., Napolitano, E., Enzo, S.,
694 2011. A multi-technique approach by XRD, XRF, FT-IR to characterize the diagenesis of dinosaur
695 bones from Spain. Palaeogeography, Palaeoclimatology, Palaeoecology, 310, 92-107.

696 Pirlet, H., Wehrmann, L.M., Brunner, B., Frank, N., Dewanckele, J., van Rooij, D., Foubert, A.,
697 Swennen, R., Naudts, L., Roone, M., Cnudde, V., Henriet, J.P., 2010. Diagenetic formation of
698 gypsum and dolomite in a cold-water coral mound in the Porcupine Seabight, off Ireland.
699 Sedimentology 57, 786–805.

700 Pueyo, J.J., Chong, G., Jensen, A., 2001. Neogene evaporites in desert volcanic environments:
701 Atacama Desert, northern Chile. Sedimentology, 48, 1411-1431.

702 Rustichelli, A., Di Celma, C., Tondi, E., Baud, P., Vinciguerra, S., 2016. Fibrous gypsum veins as
703 diffuse features and within fault zones: the case study of the Pisco Basin (Ica desert, southern Peru).
704 Journal of the Geological Society, London, 173, 405-418.

705 Smith, C. R., Glover, A. G., Treude, T., Higgs, N. D., & Amon, D. J., 2015. Whale-Fall
706 Ecosystems: Recent Insights into Ecology, Paleoecology, and Evolution. Marine Science,7, 571-
707 596.

708 Stucchi, M., Emslie, S.D., Varas-Malca, R.M., Urbina, M., 2015. A new late Miocene condor
709 (Aves, Cathartidae) from Peru and the origin of South American Condors. Journal of Vertebrate
710 Paleontology, 35, e972507.

711 Stewart, R. B. 1930. Gabb's California Cretaceous and Tertiary lamellibranchs. Academy of Natural
712 Sciences of Philadelphia Special Publication, 3, 1-314.

713 Stucchi, M., Varas-Malca, R.M., Urbina, M., 2016. New Miocene sulid birds from Peru and
714 considerations on their Neogene fossil record in the Eastern Pacific Ocean. Acta Palaeontologica
715 Polonica, 61, 417-427.

716 Thornburg, T.M., Kulm, L.D., 1981. Sedimentary basins of the Peru continental margin: structure,
717 stratigraphy, and Cenozoic tectonics from 6ºS to 16º latitude. In Nazca plate: crustal formation and
718 Andean convergence (Kulm, L.D., Dymond, J., Dasch, E.J., Hussong, D.M., eds). Geological
719 Society of America, Memoir 154, 393-422

720 Trueman, C.N., 1999. Rare earth element geochemistry and taphonomy of terrestrial vertebrate
721 assemblages. Palaios, 14, 555–568.

722 Trueman C. N. G., Behrensmeyer A. K., Tuross N., Weiner S., 2004. Mineralogical and
723 compositional changes in bones exposed on soil surfaces in Amboseli National Park, Kenya:
724 diagenetic mechanisms and the role of sediment pore fluids. J. Archaeological Science, 31, 721–
725 739.

726 Vasconcelos, C., McKenzie, J.A., Bernasconi, S., Grujic, D. and Tiens, A.J., 1995. Microbial
727 mediation as a possible mechanism for natural dolomite formation at low temperatures. Nature, 377,
728 220–222.

729 Yoshida, H., Ujihara, A., Minami, M., Asahara, Y., Katsuta, N., Yamamoto, K., Sirono, S.,
730 Maruyama, I., Nishimoto, S., and Metcalfe, R., 2015. Early post-mortem formation of carbonate
731 concretions around tusk-shells over week-month timescales: Scientific Reports, 5, 14123, doi:
732 10.1038 /srep14123.

733

734

735

736 **Figure captions**

737

738 Fig. 1. Geological and stratigraphic framework for the studied fossil specimens: geological sketch
739 map with location of CLQ and schematic stratigraphic section measured at CLQ, expanded to show
740 the position of the studied fossil vertebrates in the fossil-rich stratigraphic interval (modified from
741 Bianucci et al., 2016a).

742

743 Fig. 2. Fossil vertebrate remains and associated mollusks in the field at CLQ. A. Skull and mandibles
744 of the mysticete specimen M50. B. Detail of the endocranial nodule of M50. C, D. Mollusks in life
745 position with disarticulated but associated vertebrae of the cetacean specimen C46. E, F. Detail of
746 mollusks in life position near the bones of C46. G, H. Mollusk filled by gypsum near the cetacean
747 specimen C47.

748

749 Fig. 3. A. Mollusk valve GB38 (associated with the cetacean specimen O7) with microdrilling hole
750 (arrow); the internal cavity of the bivalve is filled by lithified sediment. B. Mollusks GB35 and GB36
751 (associated with the cetacean specimen C46). C. Mollusk specimen GB35 (associated with the
752 cetacean specimen C46) after sectioning, showing the complex internal filling structure and the
753 external Mn concentrations; the dotted line highlights the fibers of gypsum bending where touching
754 the pre-existing nodule. D. Manganese concentrations out of a mollusk specimen, cut by a gypsum
755 veinlet. E. Example of gypsum veins.

756

757 Fig. 4 A. B. SEM-BSE images at different scale of the cortical bone tissue of a rib of the cetacean
758 specimen C47, sectioned orthogonally to elongation. In B the external part of the bone shows
759 microborings. The tissue weakened by microborings was probably more prone to mechanical
760 erosion and thus it is only partially preserved. C. SEM-BSE image of the internal nodule of mollusk
761 specimen GB34, consisting of finely crystalline dolomite and scattered biogenic and detrital
762 fragments. D. EDS spectrum (raster window analysis) of the dolomite concretion in C (above) and
763 of the Mn-bearing concretion of the same specimen (below).

764

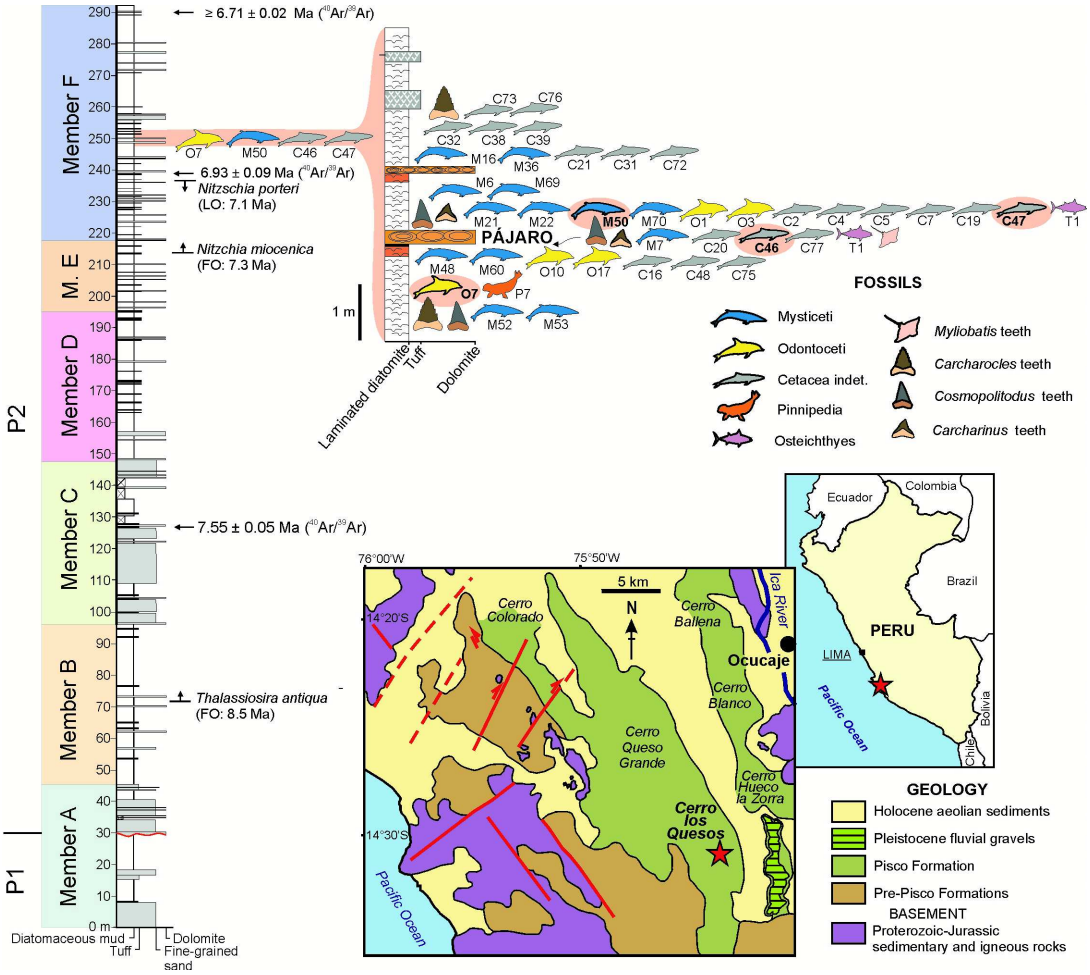
P2
P1
Member F
M. E
Member D
Member C
Member B
Member A
≥ 6.71 ± 0.02 Ma (40Ar/39Ar)
6.93 ± 0.09 Ma (40Ar/39Ar)
Nitzschia porteri
(LO: 7.1 Ma)
Nitzchia miocenica
(FO: 7.3 Ma)
7.55 ± 0.05 Ma (40Ar/39Ar)
Thalassiosira antiqua
(FO: 8.5 Ma)
PÁJARO
1 m
Laminated diatomite
Tuff
Dolomite
FOSSILS
Mysticeti
Odontoceti
Cetacea indet.
Pinnipedia
Osteichthyes
Myliobatis teeth
Carcharocles teeth
Cosmopolitodus teeth
Carcharinus teeth
Diatomaceous mud
Tuff
Dolomite
Fine-grained sand
Ecuador
Colombia
Brazil
PERU
LIMA
Bolivia
Chile
Pacific Ocean
76°00'W
75°50'W
14°20'S
14°30'S
5 km
N
Cerro Colorado
Cerro Ballena
Ica River
Ocucaje
Cerro Blanco
Cerro Queso Grande
Cerro Hueco la Zorra
Cerro los Quesos
GEOLOGY
Holocene aeolian sediments
Pleistocene fluvial gravels
Pisco Formation
Pre-Pisco Formations
BASEMENT
Proterozoic-Jurassic sedimentary and igneous rocks

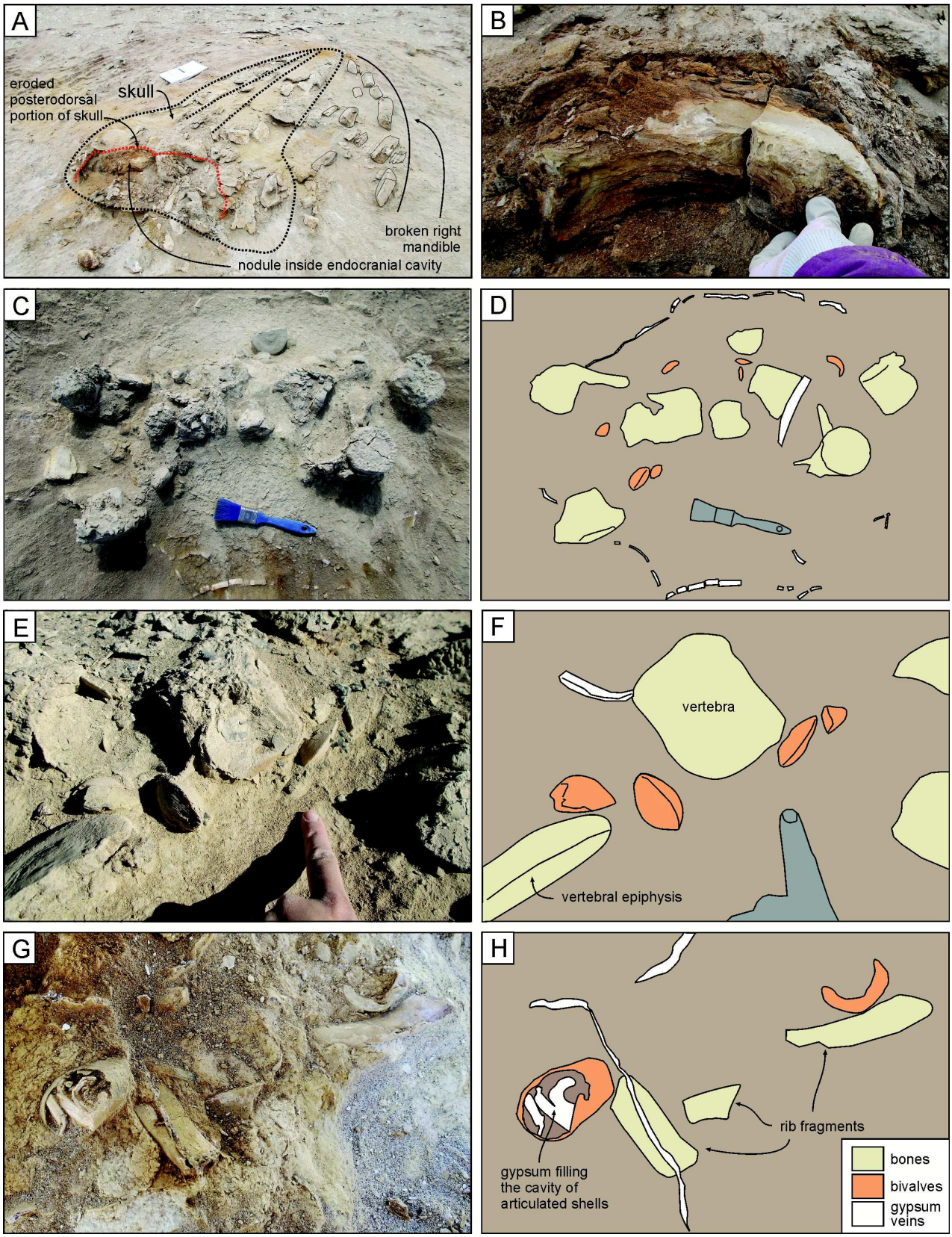
A
eroded
posterodorsal
portion of skull
skull
broken right
mandible
nodule inside endocranial cavity
B
C
D
E
F
vertebra
vertebral epiphysis
G
H
rib fragments
gypsum filling
the cavity of
articulated shells
bones
bivalves
gypsum
veins

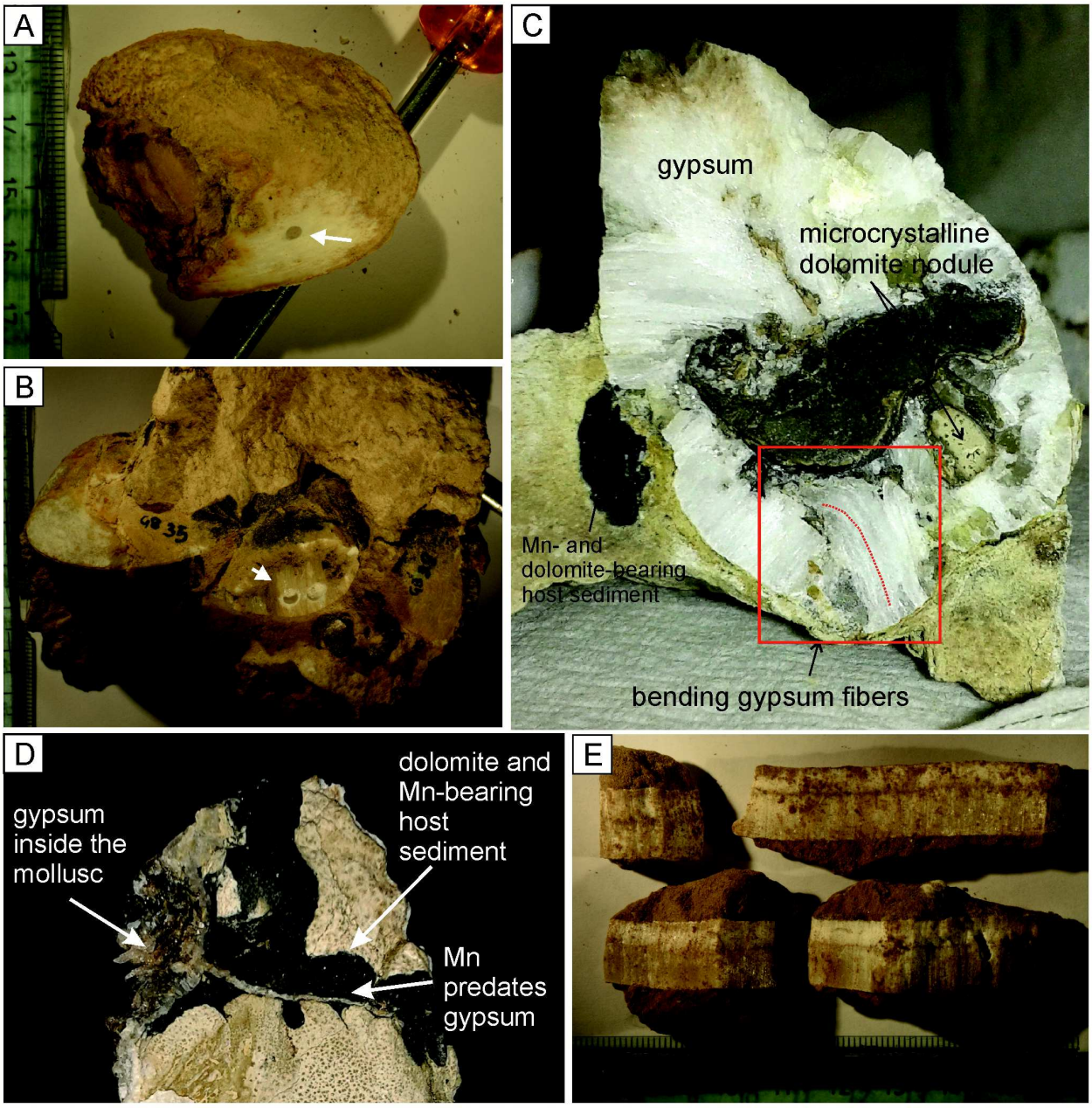
A
B
C
gypsum
microcrystalline
dolomite nodule
Mn- and
dolomite-bearing
host sediment
bending gypsum fibers
D
gypsum
inside the
mollusc
dolomite and
Mn-bearing
host
sediment
Mn
predates
gypsum
E

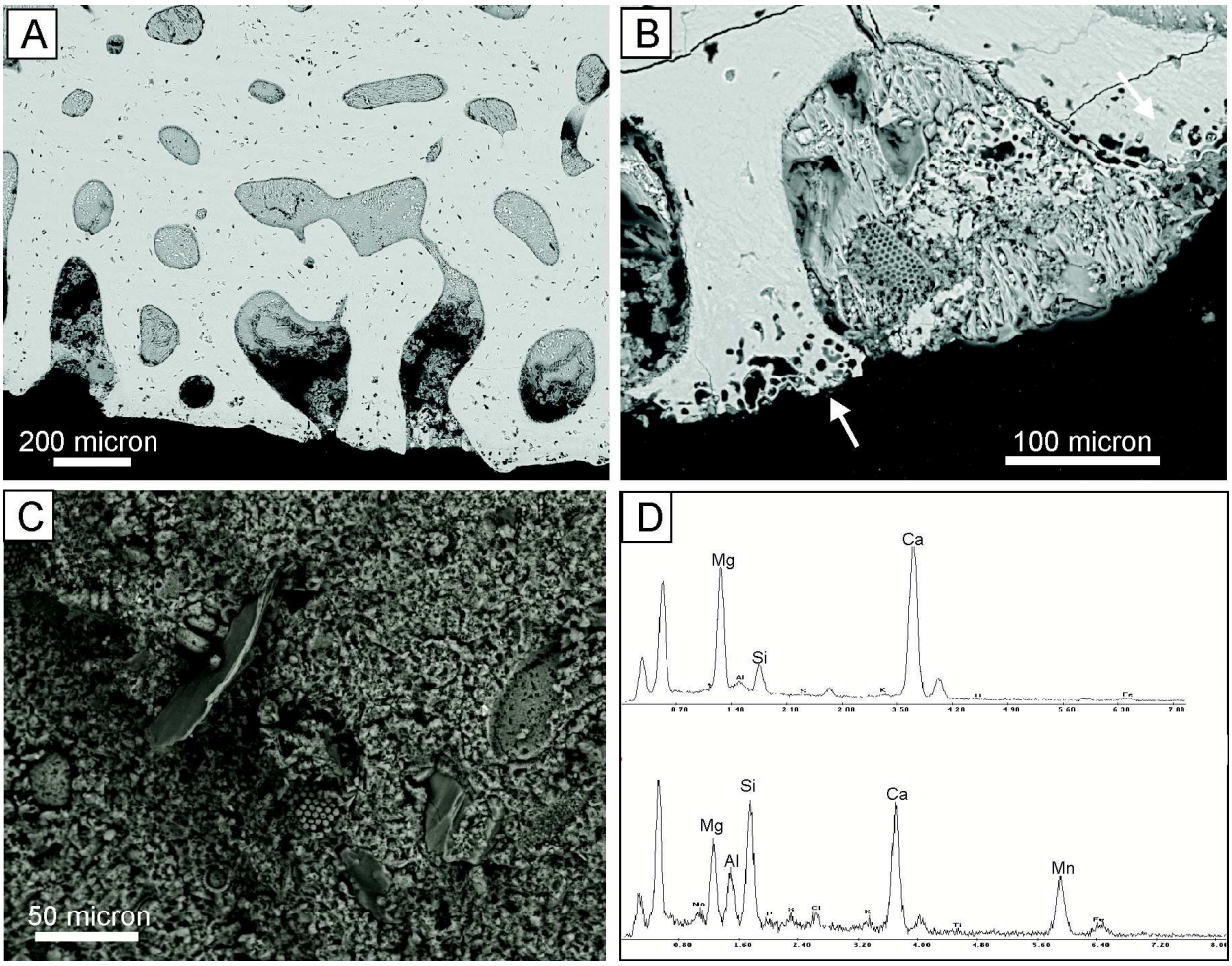
A
200 micron
B
100 micron
C
50 micron
D
Mg
Si
Ca
Si
Mg
Al
Ca
Mn

Table 1. Fossil vertebrate specimens list, with geographical coordinates, identification, summarized taphonomic features, and the mollusk and vein samples in correspondence of each of them.

Fossil specimen[1]	*Geographical coordinates*	*Systematic determination*	*Short description and field taphonomic features*	*Host sediment*	*Field evidence of early diagenetic processes*[2]	*Sample*	*Sample short description*	*Reference to figures*
O7	14° 31' 30.4" S 75° 42' 56.6" W	Phocoenidae indet.	Disarticulated but associated skeleton of an immature (unfused epiphyses of vertebrae) phocoenid consisting of a fragment of skull (rostrum), several vertebrae and rib fragments; incompleteness and breakings partially due to recent erosion.	diatomaceous mudstone	no external concretion; no Fe-Mn-rich boundary	O7-GY	vein of fibrous gypsum, 1 cm thick	Fig. 3A, E
						GB38A	gypsum-replaced bivalve shell, outer part	
						GB38B	gypsum-replaced bivalve shell, interior part	
M50	14°31'29.4" S 75°42'55.4" W	Misticeti indet.	Skull and articulated mandibles upside down of a relatively small balaenopterid (bizygomatic width: 1.5 m: estimated body length: ca 13 m): specimen partially destroyed by recent erosion.	diatomaceous mudstone	dolomite concretion filling cranium, with Fe-Mn concentrations; no external concretion; no Fe-Mn-rich boundary	GB47	gypsum-replaced bivalve shell	Figs. 2A, 2B
C46	14° 31' 19.2" S 75° 43' 00.6" W	Cetacea indet.	Several disarticulated but associated lumbar and caudal vertebrae of an immature (unfused epiphyses) small size cetacean.	lithified diatomaceous mudstone	no external concretion, but hard sediment; minor dolomite within bone porosity and as interior mold of bivalves; traces of a Fe-Mn-rich boundary	GY3	vein of fibrous gypsum, 1.5 cm thick	Figs. 2C, D, E, F; 3B, C; 4C
						GB30	dolomite inner mold of a gypsum-replaced bivalve	
						GB35	bivalve replaced and filled by fibrous gypsum, shell outer part	
						GB36	bivalve replaced and filled by fibrous gypsum, interior	
C47	14° 31' 29.9" S 75° 42' 56.1" W	Cetacea indet.	Several disarticulated but associated vertebrae and ribs of an adult (fused epiphyses) small size cetacean; one tooth belonging to a juvenile *Cosmopolitodus hastalis* shark was found near the ribs.	diatomaceous mudstone; volcanic ash just below the specimen	no external concretion; traces of a Fe-Mn-rich boundary	C47-GY	vein of fibrous gypsum, 0.5-1 cm thick	Figs. 2G, H, 4A, 4B
						GB45A	bivalve filled by fibrous gypsum, outer part	
						GB45B	bivalve filled by fibrous gypsum, interior	

(1) see Bianucci et al. (2016a); (2) we considered field evidence of early diagenetic processes, related to the decay of the whale organic matter, the presence of dolomite concretions and of concentrations of iron and manganese (= redox-dependent elements).

Table 2. XRPD results of the analyses of the post-burial minerals collected in correspondence of the selected vertebrates.

Fossil specimen	*sample*	*description*	*diagenetic/vein minerals*	*detrital minerals*
O7	C07-GY	*vein*	gypsum, anhydrite	
	GB38A	*shell*	gypsum, traces of anhydrite	quartz
	GB38B	*inner mold*	gypsum, anhydrite	
M50	GB47	*shell*	gypsum, anhydrite	quartz
C46	GY3	*vein*	gypsum, anhydrite	quartz
	GB30	*inner mold*	dolomite	
	GB35	*shell*	gypsum, minor anhydrite	
	GB36	*inner mold*	gypsum, traces of anhydrite	traces of quartz
C47	C47-GY	*vein*	gypsum, anhydrite	quartz
	GB45A	*shell*	gypsum	
	GB45B	*inner mold*	gypsum	

Table 3. Sr isotope composition of the post-burial minerals collected in correspondence of the selected vertebrates.

Fossil specimen	*Sample*	$^{87}Sr/^{86}Sr$	*abs. error**
O7	O7-GY	0.711110	0.000008
	GB38A	0.708582	0.000007
	GB38B	0.708650	0.000008
M50	GB47	0.708645	0.000009
C46	GY3	0.708644	0.000009
	GB30	0.708992	0.000008
	GB35	0.708925	0.000007
	GB36	0.708587	0.000009
C47	C47-GY	0.708766	0.000007
	GB45A	0.708714	0.000009
	GB45B	0.709060	0.000009

*in-run statistics at 2-s confidence level